Ionian Abyssal Plain: A window into the Tethys oceanic lithosphere

Anke Dannowski[1], Heidrun Kopp[1,2], Frauke Klingelhoefer[3], Dirk Klaeschen[1], Marc-André Gutscher[4], Anne Krabbenhoeft[1], David Dellong[3,4], Marzia Rovere[5], David Graindorge[4], Cord Papenberg[1], Ingo Klaucke[1]

5   [1] Dynamics of the Ocean Floor, GEOMAR, Helmholtz Centre for Ocean Research Kiel, Kiel, 24148, Germany
[2] Department of Geosciences, Kiel University, Kiel, 24118, Germany
[3] Géosciences Marines, Ifremer, Centre de Brest, Plouzané, 29280, France
[4] Laboratoire Géosciences Océan, IUEM, Université Brest, CNRS, Plouzané, 29280, France
[5] Institute of Marine Sciences - National Research Council, ISMAR-CNR, Bologna, 40129, Italy

10   *Correspondence to*: Anke Dannowski (adannowski@geomar.de)

Abstract. The nature of the Ionian Sea crust has been the subject of scientific debate for more than 30 years, mainly because seismic imaging of the deep crust and upper mantle of the Ionian Abyssal Plain (IAP) has not been conclusive to date. The IAP is sandwiched between the Calabrian and Hellenic subduction zones in the central Mediterranean. To univocally confirm the proposed oceanic nature of the IAP crust as a remnant of the Tethys ocean and to confute its interpretation as a strongly

15   thinned part of the African continental crust, a NE-SW oriented 131 km long seismic refraction and wide-angle reflection profile consisting of eight ocean bottom seismometers and hydrophones was acquired in 2014. A P-wave velocity model developed from travel time forward modelling is refined by gravimetric data and synthetic modelling of the seismic data. A roughly 6 km thick crust with velocities ranging from 5.1 km/s to 7.2 km/s, top to bottom, can be traced throughout the IAP. In the vicinity of the Medina Seamounts at the southern IAP boundary, the crust thickens to about 9 km and seismic velocities

20   decrease to 6.8 km/s at the crust-mantle boundary. The seismic velocity distribution and depth of the crust-mantle boundary in the IAP document its oceanic nature, and support the interpretation of the IAP as a remnant of the Tethys oceanic lithosphere formed during the Permian and Triassic period.

1 Introduction

The ongoing convergence between the African and Eurasian plates results in a highly complex tectonic setting in the central

25   Mediterranean [e.g. Faccenna et al., 2014; Barreca et al., 2016 and references therein]. The inherited palaeogeographic configuration of the domain involves a number of mobile compartments of oceanic or continental origin adding to the tectonic complexity of the region. Understanding the geodynamic evolution and the intricate interplay between continental and oceanic fragments hence requires exact knowledge of the crustal and lithospheric structures. Given its location, the Ionian Sea is a key element in reconstructing the kinematic evolution of the Central-Eastern Mediterranean [Finetti, 1982]. The lithosphere of the

30   Ionian Sea constitutes one of these mobile blocks, where the long lasting contradictions in the interpretations of the nature of the Ionian Sea crust ('oceanic' vs. 'thinned continental') result from a lack of conclusive imaging of the deep crust and upper

mantle, inhibiting an univocal characterization. Of special difficulty is the Messinian evaporite unit, which massively impedes seismic energy penetration and hence limits the data quality of geophysical imaging methods. The challenges in imaging have ignited a long-standing debate about the deeper structure and the nature of the crust and lithosphere of the Ionian Abyssal Plain (IAP). The interpretations range from continental or hyperextended continental lithosphere [Finetti and Morelli, 1973;

5   Cloething et al., 1980; Baldi et al., 1982; Makris et al., 1986; Ferrucci et al., 1991; Cernobori et al., 1996; ==Mantovani et al., 2002;== Hieke et al., 2003; Roure et al., 2012] to oceanic or atypical oceanic lithosphere [Finetti, 1981; 1982; Makris et al., 1986; Leister et al., 1986; De Voogd et al., 1992; Finetti et al., 1996; Faccenna et al., 2001; 2004; Catalano et al., 2001; Finetti, 2003; Gallais et al., 2011; 2012; Speranza et al., 2012; Dellong et al., 2018].

Finetti [1982] used geological, geophysical and drilling exploration data to infer that the crust in the IAP is of oceanic type

10   adjacent to continental crust. The IAP was interpreted to consist of oceanic type crust by a two-ship deep refraction and reflection seismic experiment [De Voogd et al., 1992]. Oceanic crust east of the Malta Escarpment is inferred from CROP-lines M23A and M3 [Finetti, 2003]. Furthermore, time and pre-stack depth migrated reflection seismic data [Gallais et al., 2011; 2012] and magnetic anomaly data [Speranza et al., 2012] indicated oceanic crust within the IAP. Contrasting interpretations are based on echo sounding and seismic reflection data [Hieke et al., 2003] and a paleo-geographic analysis of

15   faults [Roure et al., 2012], interpreting the crust of the IAP to be of continental type. While the majority of studies today infer an oceanic type crust in the IAP [LeBreton et al., 2017; Dellong et al., 2018], robust information on the crustal structure of the IAP including Moho depth and seismic velocities to confirm the oceanic nature of the crust are still sparse.

To fill this gap, RV Meteor cruise M111 in 2014 targeted the crustal and lithospheric structure of the Ionian Abyssal Plain (Fig. 1). Along line DY-05, modern seismic refraction and wide-angle reflection data were acquired using four ocean bottom

20   seismometers (OBS) and four ocean bottom hydrophones (OBH). The aim of this work is to provide information on the seismic velocity distribution and crustal structure to ~~confirm~~ the nature of the crust in the IAP.

2 Geological Setting

The Ionian Sea and its abyssal plain are sandwiched between the Calabrian and Hellenic subduction zones in the central-~~eastern~~ part of the Mediterranean basin (Fig. 1). The IAP comprises an asymmetric basin of approximately 600 km length and

25   330 km width with water depth reaching ~4000 m in its central part. Its lithosphere is actively subducting underneath Eurasia along both subduction zones (Calabrian to the north and ~~Western Mediterranean Ridge~~ to the east), causing a high potential for devastating earthquakes and tsunamis. Both subduction zones are characterized by large accretionary prisms, which have advanced into the Ionian Sea and cover vast parts of the IAP. Imaging of the IAP crust is difficult because of the voluminous sedimentary cover of the accretionary prism [Dellong et al., 2018], which furthermore is underlain by a thick sequence of

30   Messinian evaporites [Ryan et al., 1982]. Only a relatively small 'window' of approximately 100 km length and 60 km width remains undisturbed by the highly deformed accreted sequences advancing from the north and east or by the Medina seamount cluster of volcanic origin found to the south [Finetti, 1982]. To the south and west, the Ionian Sea is bound by the continental

platforms of Libya and the Malta-Hyblean plateau, respectively. The ~~gradation~~ from the deep-ocean environment of the IAP to the shallow water carbonate platform of the continental Malta-Hyblean plateau is marked by the Malta Escarpment. This distinct, 290 km long and 3.2 km high scarp is an inherited transform margin from the early Mesozoic [Argnani and Bonazzi, 2005; Micallef et al., 2016; Dellong et al., 2018] that traces the transition from the oceanic domain of the Ionian Sea to the
5   Tertiary-Quaternary continental foreland domain of the Pelagian platform [Barreca et al., 2016].

Direct sampling of the sediment cover is available from ODP/DSDP sites [Ryan et al., 1973], while sub-basement structure was mainly inferred from potential field and refraction data. Early studies [Locardi and Nicolich, 1988; Nicolich, 1989; De Voogd et al., 1992; Scarascia et al., 1994] considered the crust to be 15-20 km thick. Later investigations refined this value to
10   8-10 km [Catalano et al., 2001; Gallais et al., 2011; Dellong et al., 2018]. Important insight has come from heat flow measurements, which revealed that very low values prevail in the eastern Mediterranean compared to the western Mediterranean [Jiménez-Munt et al., 2003], indicating distinct differences in the age and thickness of the lithosphere in these realms (younger, warmer lithosphere in the west; older, colder and thicker lithosphere in the east). Low heat flux values of 30-40 mW/m2 [Della Vedova and Pellis, 1989] from the Ionian basin underpin its oceanic origin of at least Mesozoic age, coherent
15   with the Pangea breakup and rifting of the Tethys ocean during the late Paleozoic or Early Mesozoic ~~[Sage et al., 1997; Stampfli et al., 2002; Agard et al., 2011]~~. In addition, the relatively high Bouguer gravity anomaly of the IAP with values exceeding 200 mGal [Morelli et al., 1975] suggests a shallow Moho boundary [Dellong et al., 2018]. The seafloor magnetic pattern of the IAP indicates that the Ionian Sea lithosphere was formed around 220-230 Ma during Triassic times and it is considered as a remnant of the Tethys ocean [Speranza et al., 2012].

The nature of the Ionian lithosphere and the structure of the Ionian crust ~~are not only of regional interest, but on a wide scale, as they~~ are crucial to the understanding of the collisional and subduction dynamics of the entire ~~central~~ Mediterranean. In particular, the Tethyan affinity of the Ionian lithosphere and its oceanic nature support the hypothesis that the Adriatic microplate, which comprises the Ionian Sea in its southernmost portion, was a rigid promontory of Africa [e.g. Channell et al.,
25   1979; Dewey et al., 1989]. However, thrust faulting and inversion structures in the IAP as interpreted from seismic data [Gallais et al., 2011, 2012; Polonia et al., 2011, Roure et al., 2012] are indicative of active deformation of the Ionian crust, which would contradict a 'rigid' connection to Africa ~~[LeBreton et al., 2017]~~ and support the idea of an independent Adria micro-plate.

3 Data and methodology

During RV Meteor cruise M111 wide-angle refraction seismic data were acquired simultaneous to reflection seismic data.
30   Profile DY-05 is 84 nm long and crosses the Ionian Sea basin from SW to NE (red line in Fig. 1). The location of the line was chosen to cover the area of the IAP that is neither affected by the emplacement of volcanic structures (Medina Seamounts in the south) nor affected by the advancing thick accretionary prisms of deforming sediment in the north and east in order to gain

an 'unobstructed view' into the deep IAP crust and lithosphere. The central part of the profile was covered by eight seafloor stations (OBH501 - OBS508) with a spacing of 4 nm. Shooting (946 shots) was extended for ~ 20 nm beyond the first and last instrument, respectively, in order to record long offsets from shots travelling through the subsurface. An airgun array consisting of 6 G-gun clusters with a total volume of 84 l (5440 cu.in.) at 210 bar was fired at a 60 s shot interval. Data quality was very

5 good and arrivals were recorded over the entire profile length. Mantle phases, PmP reflections and Pn phases, were recorded on all stations. A mini-streamer with 4 channels spread over an active length of 65 m was towed at a depth of 8 m between the airguns. For each channel, 6 hydrophones with a distance of 0.5 m were grouped together. The streamer served two purposes: it was used to control the correct functioning of the air guns and provided information on the uppermost sedimentary structures in regions where seafloor roughness does not cause aliasing. A medium gun delay of 78 ms could be identified, while one gun

10 firing out of sequence, as recognized on the streamer data near trace 800 in Figure 2.

3.1 Description of the multichannel seismic reflection data

The stacked MCS data section displays the upper subsurface structure in two-way travel time (twt; Fig. 2). The water depth along the profile increases from ~3600 m at the southern termination in the vicinity of the Medina seamounts to 4090 m in the central portion of the profile. The water depth declines again towards the northern end of the line which starts to cover the

15 Ionian accretionary prism (compare Fig. 1). North of the rough seafloor of the Medina Seamounts group, the data section is dominated by the thick sedimentary and evaporitic sequences which fill the basin. Stratified sediment layers are softly inclined along the southern part of the profile, between shot numbers 150-450. Towards the centre of the basin, horizontally layered, sub-parallel sequences are onlapping onto these strata between shots 450-550. These units are underlain by a thick sequence of incoherent amplitudes truncating the sediment layers in the south. A prominent strong amplitude reflector may be traced

20 from shot point 150 at 5.2 s to around shot number 550 at 5.7 s. Whereas a coherent layering is visible in the units above this reflector, the units below are seismically much more opaque. The base of these units is marked by a strong negative reflector at 5.5 s (near trace 200) to 6.3 s (near trace 800). Below this reflector, the seismic signal is strongly attenuated and no coherent structures may be identified. Two deep reflectors to the north at 6.7 s and 7.1 s lose their seismic amplitude coherence beyond shot numbers 550 and 750, respectively.

25 **3.2 Description of the seismic wide-angle reflection and refraction data**

Figure 3 presents seismic shot sections, including picked and calculated travel time picks, of the two outermost stations, OBH501 and OBS508. The earliest arrival at the stations is the direct wave through the water picked in yellow (PDirect, phase 1). Magenta picks (PsPTopME, phase 3) represent the base of the youngest sediment units. The geometry of these sediment layers is well imaged in the multi-channel seismic data (Fig. 2) by a strong positive reflector (PsPTopME). Red picks (PsME,

30 phase 2) follow the first arrivals to an offset of ~15 km (3.5 to 4.5 s), representing refracted waves travelling through the evaporite layers with an apparent velocity of 4.5 km/s. At about 15 km offset from the station, at the limit of the red picks (phase 2), a prominent shadow zone indicates a strong negative velocity inversion in the subsurface including a thick low

velocity zone. The near-offset early arrivals are offset by 1.5 s to the deeper crustal first arrival phases (dark green picks), that have been recorded starting at roughly 6 s. A strong negative reflector starting at zero offset is present on all OBS record sections and is picked in blue (PsPBotME, phase 5). It marks the base of the Messinian unit at ~3.6 s at zero offset. After a ~1.4 s long sequence of high amplitude reflectors follows a low-frequent high-amplitude reflector (light green, PsPTopAU,

5   phase 7), visible between 0 to 20 km offset at ~5 s. Underneath a second similar reflector is picked in magenta (PbP, phase 9) at ~5.6 s. These two reflectors originate from the base of the slow sediment unit and the basement, respectively. At larger offsets, two crustal phases (violet (Pb, phase 8) and green picks (Pg, phase 10)) could be identified. At about 35-40 km the onset of the mantle reflection is observed and picked in light blue (PmP, phase 11) and mantle refracted phases in bright red (Pn, phase 12).

10   **3.3 Methodology and modelling strategy**

The analysis of profile DY-05 targeted the structure of the crust by developing a velocity model for the sedimentary strata, the crust and the uppermost mantle. This was achieved by forward modelling of the observed travel times using the raytracing software RAYINVR [Zelt and Smith, 1992; Zelt and Forsyth, 1994]. It runs on the graphical user interface MODELING [Fujie et al., 2008]. Travel times were picked using the software PASTEUP [Fujie et al., 2008]. Attempts to apply tomographic

15   inversion approaches failed due to the presence of a thick low velocity zone. The final forward model (Fig. 4) was developed starting with the water layer and progressing downward layer by layer. The geometry of the upper layers was constrained by the MCS data (Fig. 2). The geometry of the deeper layer boundaries was optimised by using the inversion algorithm of RAYINVR. The RMS misfit and the Chi2 value for each phase are provided in Table 1.

To corroborate the seismic velocity model gained by seismic travel time forward modelling, complementary two-dimensional

20   gravity forward modelling was performed. Especially at the profile ends with only moderate station coverage, the seismic velocity model is highly uncertain and gravity modelling (Fig. 5) helps to constrain and adjust the model. The free-air anomaly (FAA) along the 2-D profile was extracted from satellite altimetry data [Sandwell & Smith, 1997]. Based on the seismic velocities an initial 2D density model was constructed. The model response [Talwani et al., 1959] was compared to the observed free-air anomaly data along the profile. Minor adjustments to the model densities, all within common density-velocity

25   relationships [Carlson and Herrick, 1990; Christensen and Mooney, 1995], were applied to achieve a reasonable fit between calculated and observed FAA.

To validate the forward modelling, synthetic data based on the final seismic velocity model were calculated and compared to the recorded data (Fig. 6).

30

4 Interpretation and Results

4.1 Shallow structures from multi-channel seismic data

The uppermost unit in the MCS data was drilled at DSDP site 374 [Hsü et al., 1978] and corresponds to Plio-Quaternary sediments. The lower limit of this unit is marked by the so-called A-reflector [Finetti and Morelli, 1972], which forms the

5   transition to the Messinian evaporite layers [Hsü et al., 1978; Gallais et al., 2011]. This reflector corresponds to phase 3 (magenta picks) in the seismic sections of the OBH (Fig. 3).

The base of the Messinian evaporites has been termed the B-reflector by Finetti and Morelli [1972]. Phase 5 (blue picks) in the OBS seismic sections (Fig. 3) corresponds to this reflector. The B-reflector disappears in our seismic section near trace 800 towards the north. The two reflectors identified between traces 550 and 750 at 6.6 s and 7.2 s indicate Pre-Messinian

10   sedimentary layering. We link these reflectors to Tortonian age, as identified by Gallais et al. [2011] in the crossing seismic line Arch21 (Fig. 1).

At trace 100 the layering of the upper sediments is disturbed by the volcanic signature of the Medina Seamounts. In the northern part of the profile, starting near trace 570 (OBH503), the A-reflector of the Messinian unit disappears gradually towards the northern profile end. The Plio-Quaternary sediment layering above, near trace 700, is characterized by gently undulating folds.

15   Near trace 880, the stratification of the Plio-Quaternary sediments disappears completely and anal folds can be observed at the surface. We interpret these observations as signatures of the deformation front of the Calabrian accretionary wedge, expressed at different depth levels. The deformation of the sediments possibly creates fluid pathways and thus may support the dissolution of the evaporites below.

4.2 Shallow and deep structures from seismic travel time modelling

20   Layer 1 in our final velocity model (Fig. 4a) is 250-500 m thick with rapidly increasing seismic velocities from 1.8 km/s to 2.2 km/s, top to bottom. From drilling it is known that L1 is composed of unconsolidated Plio-Quaternary sediments [*Hsü et al.*, 1978]. The underlying layer L2 is characterized by uniform seismic velocities of 4.4 km/s to 4.65 km/s and a thickness of 0.8 km to 1.3 km. L2 is interpreted as the Messinian evaporite unit (Layer 2 in Figure 4a). The A-reflector and the reversed polarity B-reflector occur as strong phases in the OBS data at all stations, representing the top and bottom of the Messinian

25   evaporite unit, respectively. The B-reflector at the base of the Messinian unit is also known as S1-horizon from the ESP5 (Expanding Spread Profile) study by *De Voogd et al.* [1992].

Below the B-reflector, the OBS data show a succession of high-amplitude reflectors similar to observations made by *Gallais et al.* [2011] in the MCS data (Archimede and PrisMed01 profiles). However, it is difficult to link these reflectors to certain horizons in our velocity model; thus, we modelled the Pre-Messinian sediments as a low velocity layer (layer 3 in Figure 4a)

30   with velocities increasing from 3.1 km/s at the B-reflector to 3.7 km/s at the base of the unit. *Gallais et al.* [2011] propose that the upper part of the unit, containing the succession of reflectors, is of Tortonian age, overlying an undifferentiated Tertiary sequence and Mesozoic sediments. From 20 km towards south, we observe higher velocities up of 3.7 – 4.7 km/s (top to

bottom) that we relate to the Medina Seamounts. This part of the profile, however, was not covered by OBS stations; thus, the model here is less reliable.

A high-amplitude, low frequency reflector marks the top of layer 4 (Figures 3 and 4a), that shows a low velocity gradient, with seismic velocities of 4.8-4.9 km/s. We interpret L4 as a sediment unit, based on the seismic velocities and the velocity

5   gradient within the layer. Thus, we observe the crystalline basement at a depth of ~9.5 km, at OBH501, to ~8.5 km, at OBS508. Indeed, layer 5 (Fig. 4a) shows a steeper velocity gradient to a depth of ~11 km. The seismic velocities increase from 5.1 km/s to 6.4 km/s, typical for seismic layer 2 in upper oceanic crust. The upper crust is approximately 2-3 km thick. Layer 6 (Fig. 4a) again shows a lower velocity gradient with velocities increasing from 6.4 km/s to 7.2 km/s from top to bottom, typical for oceanic crust in seismic layer 3 [*White et al.*, 1992]. Layer 7 (Fig. 4a) with velocities higher than 7.8 km/s is interpreted as

10   mantle with a seismic Moho at ~15 km depth at OBH501 and at ~17 km depth at OBS508.

In the northern part of the profile, in the IAP, 6-7 km thick crust is encountered. Towards the southern end, the crust thickens to at least ~9 km. Due to the moderate resolution at the model termination in the south, especially at greater depth, it is difficult to identify the nature of the crust in the southern part. In conjunction with crustal thickening we observe crustal velocities at the crust-mantle boundary of 6.8 km/s. The recorded seismic data show a change in the characteristics of the mantle phases

15   towards the south. This could result from a change in the nature of the crust or simply originate from the influence of the Medina Seamounts. The nature of the Medina Seamounts is not well studied, however it is proposed to be volcanic [*Finetti*, 1982].

Again, at the edges and with increasing depth modelling becomes less accurate. Pick uncertainties and data fits are presented in Table 1.

Phase	Phase Number	Number Picks	RMS [s]	Chi²	Pick uncertainty [s]
All picks		8128	0.064	0.979	
P_{Direct}	1	422	0.004	0.123	0.010
PsP_{TopME}	3	299	0.012	0.378	0.020
Ps_{ME}	2	1017	0.019	0.867	0.020
PsP_{BotME}	5	313	0.020	0.986	0.020
PsP_{TopAU}	7	985	0.072	1.054	0.070
PbP	9	919	0.078	1.239	0.070
Pb	8	424	0.089	1.637	0.070
Pg	10	1349	0.079	1.271	0.070
PmP	11	1324	0.048	0.392	0.080
Pn	12	1498	0.072	1.038	0.080

4.3 Gravity modelling

The results of the 2D gravity forward modelling are shown in Figure 5. In the south, possible 3-D effects of the Medina Seamounts have not been taken into account during the modelling. However, the seismic velocities of the crust and the density

5   of the crust decrease towards the south, roughly south of kilometre 30 of the profile. At the corresponding location in the model, a thickening of the crust is observed. A good fit is observed with a RMS deviation of 1.46 mgal. Figure 5b presents a case without the shallow density anomaly between 5 km and 20 km along the profile. The overall trend of an increasing FAA from south to north can be observed, however the short wavelength fit is inferior compared to the final model (Fig. 5a); the RMS misfit is 2.62 mgal. This part of the model is not covered by OBS resulting in less well constrained seismic velocities,

10 however, shallow denser material supports the observed higher seismic velocities. This is supported as well by the MCS data in Figure 2, where the sedimentary succession is deformed. To further test the velocity model, a constant crustal velocity was assumed. In contrast to the final model densities in the crust were defined with constant values typical of oceanic crust over the entire profile (Fig. 5c). The model response in Figure 5c shows a strong misfit between observed and calculated FAA south of km 60 (13.92 mgal). In this scenario, the crustal densities are too high in the southern part of the model. Additionally,

15 assuming a constant crustal thickness would even enlarge the misfit of the data. By means of the gravity study, we can confirm the final seismic velocity model, even for the portions not covered by OBS.

4.4 Synthetic data

The computation of synthetic data serves to ~~validate~~ the forward modelling results. The upper panel of Figure 6a shows the synthetic seismogram of OBH501 based on the final velocity model (Fig. 4). The synthetic seismogram was computed by

20 means of a 2-D finite difference scheme for the solution of the elastic isotropic wave equation [Hestholm et al., 1994]. The input velocity model had a grid cell size of 50 m. The seismogram was computed with a P-wave source frequency up to 30 Hz, while a 2 ms time step was chosen. No random noise was added. The gross features of the observed amplitudes (Fig. 6b) could be reproduced in the synthetic record section (Fig. 6a). The ~~near offset~~ waveforms of the evaporite unit show high amplitudes that rapidly decrease with offset. The large shadow zone is caused by a thick unit of sediment layers with slower

25 seismic velocities compared to the evaporite unit. This portion of the model was kept simple during forward modelling; thus, we observe a lack in phases between 4 s and 5 s in the synthetic data compared to the observed data in Figure 6b. The additional phases in the observed data indicate internal layering of the evaporite unit as well as layering within the slow sediment unit, which were not resolved during travel time modelling. At roughly 5 s the reflected phase of the fast sediment unit above the basement as well as the reflection of the basement at 5.5 s are present in the synthetic data with weak amplitudes (Fig. 6a).

30 The crustal phases between 15 km and 30 km become stronger again, while the PmP, between 40 km and 50 km, shows high amplitudes. This feature ~~is observed in the recorded data as well and~~ is associated with a discontinuity at the crust-mantle

boundary. The mantle phases with offsets larger than 55 km slowly fade. They can be better recognised in the synthetic data where they are not obscured by ambient noise. The apparent velocities of the main features fit the observed data.

5 Discussion

5.1 Deformation ~~and tectonic thickening~~

~~Different deformation fronts~~ have been observed at different depth levels (Fig. 2), however, we do not interpret this as a result of deformation stepping back in time towards the north. We rather interpret the scenario as deformation that happens at all three depth levels simultaneously, caused by the distributed thrusting in the toe of the Calabrian accretionary wedge. The distribution of the deformation fronts is most likely a function of the rheological properties of the different layers. In fact, we observe distributed shortening and tectonic thickening of the Messinian salt unit, resulting in an unclear and chaotic A-reflector within short distance towards the north. While the Plio-Quaternary sediments at greater depth show gently undulating folds, the deformation front at the surface is expressed by a sudden occurrence of distinct anticlinal folds. The thickness of the Plio-Quaternary sediments is rather constant (Fig. 2 and 4) supporting the idea that rheological properties influence the location of the deformation front at each layer. The MCS profile Crop-M2 [Polonia et al., 2011] crosses the DY-05 profile at OBH501 (Fig. 7a). They interpreted the base of the Messinian evaporites as the detachment, acting as the plate boundary between the post-Messinian wedge (Eurasia) and pre-Messinian sediments on top of the very old African subducting oceanic crust. This would indeed be consistent with our observations of a B-reflector that can be traced through almost the entire profile.

5.2 Pre-Messinian sedimentary layers

Beneath the B-reflector, the seismic signal is strongly attenuated, both, in the OBS and MCS data. In the MCS data, short reflective bands can be observed, indicating Pre-Messinian sedimentary layering. The OBS data show a sequence of steep angle reflections with high frequencies. However, a comparison of OBS and MCS data proved unsuitable to correlate the observed phases at the different stations. The gained model in this portion is highly unreliable, especially the velocity information with absolute velocities and the velocity gradient.

Layer 4 was the next layer that could be verified by a high-amplitude, low frequency reflector. Based on the absolute velocity and the low velocity gradient it is interpreted as a sedimentary layer. While De Voogd et al. [1992] interpreted layer 4 (Fig. 4a) as oceanic upper crust ~~layer 2A,~~ we interpret this to be a 1 km thick layer of carbonate sediments (Fig. 7b). For seismic layer 2 of oceanic crust, we would expect a high velocity gradient with absolute velocities lower than observed [Spudich and Orcutt, 1980; White et al., 1992], or a low velocity gradient with higher absolute velocities for continental crust [Christensen and Mooney, 1995]. LeMeur [1997] and Gallais et al. [2011] propose that L4 represents a further sediment unit, which is supported by the imaged layered facies in their studies (compare Fig. 7c).

5.3 Nature of the lithosphere of the Ionian Abyssal Plain

Based on the seismic velocities and the gravimetric modelling we interpret the IAP to be of oceanic nature. Further south in the vicinity of the Medina seamounts, we observe a change in the characteristics of the crust towards a continental type crust. In the following discussion we will concentrate on the crust of the central IAP:

5   M111 refraction seismic line DY-05 crosses the SE end of MCS profile Crop-M2 [Polonia et al., 2011] at OBH501 in the northern IAP (Fig. 1). Both studies show coinciding results down to the crystalline basement (Fig. 7a), which is the limit of resolution for the MCS data. Polonia et al. [2011] interpreted the crust as very old African oceanic crust. The seismic results of our study are as well in good agreement with the findings of Speranza et al. [2012]. They could fit the magnetic anomaly pattern of the Ionian Sea with models consisting of a 2 km thick oceanic crust layer 2A. In our modelling we did not distinguish

10   between layer 2A and 2B, however, the total upper crustal thickness is estimated around 2-3 km. Similar to our findings, Makris et al. [1986] observed velocities up to 7.2 km/s resulting from oceanic crust, however, stations within the IAP failed and their profile could only be extended to the IAP based on shots within the IAP recorded at stations outside the IAP, leaving results with a high uncertainty in this portion of the profile. Thus, the authors could not exclude stretched continental crust with intruded upper mantle. A similar hypothesis of thinned continental crust was published by

15   Finetti and Morelli [1973] and Finetti [1981; 1982] based on gravity data, however, they could not explain the gravity data without intruded mantle material. Along the seismic profiles CROP-M23A and M3, Finetti [2003] interpreted crust east of the Malta Escarpment to be of oceanic nature, with a crystalline basement at 7 s to 8 s twt, which is in depth similar to our findings. Also Cernobori et al. [1996] observed the seismic Moho along ION6 (further north of DY-05) at 16 km depth, which coincides with our findings. They studied the northern end of the IAP using the multi-channel seismic line ION6, however, interpreted

20   the IAP as thinned continental crust. Hieke et al. [2003] presented an extensive discussion of previous work and argued that because of magnetic anomalies, missing heat flow anomalies, and the gravity data, the IAP is a thinned part of the African continental crust and Adria is then to be considered as an African promontory. We agree that the system seems to be in equilibrium regarding the heat flow, however, similar low values of 38-46 mW/M² are expected for very old oceanic crust as well [Sclater et al., 1980]. Roure et al. [2012] refute that the Ionian Basin is composed of oceanic lithosphere and put this into

25   the context of other areas nearby. The authors contradict Sioni [1996] and Gallais et al. [2011] in interpreting the high-amplitude reflector at 8 s twt (in the seismic line PrisMed01) as top of oceanic crust. However, the reflectors from OBS502 and PrisMed01 line show an ideal fit (Fig. 7c). The results of our study show that the seismic velocities are very typical for oceanic crust while being too fast for typical continental crust (Fig. 4).

Our gravity modelling (Fig. 5) shows a good data fit assuming oceanic crust for the IAP with a change in crust towards the

30   south and towards the extension of the Malta Escarpment. We argue that the observed velocity gradients of the upper crust (high velocity gradient) and the lower crust (low velocity gradient) are typical for oceanic crust. The calculated velocities (Fig. 4) are rather typical for gabbroic rocks, which also applies to the densities found in the gravity forward modelling (Fig. 5). We observe a crustal thickness of ~6 km in the north and ~9 km at the southern end of the profile.

The seismic results of our study are in good agreement with the findings of De Voogd et al. [1992] who analysed the ESP5 data from a 2-ship experiment in the vicinity of OBS502. We receive similar results for the shallow part of the models (Fig. 7b), the deeper portions vary regarding the depth of the layers. The crustal thickness at ESP5 is about 8 km versus 6 km at OBS502 along profile DY-05. The lower crust has a similar thickness for both experiments. While along DY-05, the crystalline

5   basement becomes slightly shallower towards south, the seismic Moho was found at ~15 km depth at the northern profile end, deepening to ~17 km depth at the southern profile end. We observed a seismic mantle velocity of 7.8 km/s increasing with depth, while the studies of the ESP5 experiment [De Voogd et al., 1992] (Fig. 7b) and Makris et al. [1986] show mantle velocities of 8.1 km/s and 8.5 km/s. However, both experiments recorded shots from only one side of the instruments leaving high velocity uncertainties for the deeper portions of their models.

10 The Crop-M3 profile [Polonia et al., 2011] crosses the Malta Escarpment further in the west of our study area. During RV Meteor M111 cruise, wide-angle refraction seismic data (DY-P1) were acquired along this profile, which were analysed by Dellong et al. [2018]. In a seismic travel time forward model, they observed continental crust west of the Malta Escarpment and oceanic type crust under the Calabrian accretionary wedge, supporting our findings for the IAP. Studying new marine satellite gravity maps of the area [Sandwell, 2014], we can identify the deep-seated Malta Escarpment as a transition zone

15 from continental to oceanic type crust, further south towards the Medina Seamounts. This supports our seismic and gravimetric models that indicate a change in crust towards the south, towards the Medina Seamounts.

6 Conclusions

Our new seismic velocity model images the deep subsurface of the IAP in more detail than previous approaches. In addition,

20 gravimetric modelling validates these findings. Our data indicate that the IAP is underlain by oceanic crust with seismic velocities increasing with depth from 5.1 km/s to 7.2 km/s. The thickness of the crust in the IAP is 6-7 km but thickens to ~9 km in the vicinity of the Medina Seamounts, which marks the southern boundary of the Ionian oceanic crust. At the crust-mantle boundary crustal seismic velocities decrease from 7.2 km/s in the north to 6.8 km/s in the south. We interpret the layer above the crystalline basement, earlier interpreted as layer 2a, as a unit of seismically fast sediments, possibly carbonates. This

25 is in agreement with the warm environment during the formation of the Tethys Ocean. The oceanic lithosphere of the IAP and indications of active deformation of the Ionian crust contradict a 'rigid' connection to Africa as a thinned part of the African continental crust. The crust is oceanic, thus, we consider the IAP to be a remnant of the Tethys lithosphere formed during the Permian and Triassic Period as suggested by Speranza et al. [2012], which places the African margin much further south than previously thought. Previous and recent studies of the area are combined in Fig. 8 to show the distribution of oceanic

30 lithosphere.

7 Acknowledgements

The cruise M111 of RV Meteor was funded by the Deutsche Forschungsgemeinschaft DFG with additional support from GEOMAR. Our special thanks go to the captain and crew of RV Meteor for their excellent support at sea.

References

5 ~~Agard, P., Omrani, J., Jolivet, L., Whitechurch, H., Vrielynck, B., Spakman, W., Monié, P., Meyer, B., and Wortel, R.: Zagros orogeny: A subduction-dominated process, Geological Magazine, 148(5-6), 692–725, https://doi.org/10.1017/S001675681100046X, 2011.~~

Argnani, A. and Bonazzi, C.: The Malta Escarpment fault zone offshore eastern Sicily: Pliocene-Quaternary tectonic evolution based on new multichannel seismic data, Tectonics, 24, TC4009, https://doi.org/10.1029/2004TC001656, 2005.

10 Baldi, P., Degli Angioli, E., Piallini L., and Mantovani, E.: Gravity anomaly interpretation in the Calabrian Arc and surrounding regions: a tridimensional approach, Earth Evol. Sci., 3, 243-247, 1982.

Barreca, G., Scarfì, L., Cannavò, F., Koulakov, I., and Monaco, C.: New structural and seismological evidence and interpretation of a lithospheric-scale shear zone at the southern edge of the Ionian subduction system (central-eastern Sicily, Italy), Tectonics, 35, 1489–1505, https://doi.org/10.1002/2015TC004057, 2016.

15 Carlson, R.L., and Herrick, C.N.: Densities and porosities in the oceanic crust and their variations with depth and age, J. Geophys. Res., 95, B6, 9153-9170, https://doi.org/10.1029/JB095iB06p09153, 1990.

Catalano R., Doglioni, C., and Merlini, S.: On the Mesozoic Ionian Basin, Geophys. J. Int., 144, 49-64, https://doi.org/10.1046/j.0956-540X.2000.01287.x, 2001.

Cernobori, L., Hirn, A., McBride, J.H., Nicolich, R., Petronio, L., and Romanelli, M.: Crustal image of the Ionian basin and
20 its Calabrian margins, Tectonophysics, 264, 175-189, https://doi.org/10.1016/S0040-1951(96)00125-4, 1996.

Channell, J.E.T., D'Argenio, B., and Horvath, F.: Adria, the African promontory, in Mesozoic Mediterranean palaeogeography, Earth Science Reviews, 15, 213–292, https://doi.org/10.1016/0012-8252(79)90083-7, 1979.

Christensen, N.I., and Mooney, W.D.: Seismic velocity structure and composition of the continental crust: A global view. J. Geophys. Res.: Solid Earth, 100 (B6), https://doi.org/10.1029/95JB00259, 1995.

25 Cita, M.B., Ryan, W.B.F., and Kidd, R.B.: Sedimentation rates in Neogene deep-sea sediments from the Mediterranean and geodynamic implications of their changes, in Hsü, K.J., Montadert, L. et al., Init. Rep. DSDP XLII, (part 1) 991–1002, 1978.

Cloetingh, S., Nolet, G., and Wortel, R.: Crustal structure of the Eastern Mediterranean inferred from Rayleigh wave dispersion, Earth Planet Sci. Letters, 51, 336-342, 1980.

Della Vedova, B., and Pellis, G.: New heat flow density measurements in the Ionian sea. Atti VIII Convegno GNGTS, Roma,
30 1133-1145, 1989.

Dellong, D., Klingelhoefer, F., Kopp, H., Graindorge, D., Margheriti, L., Moretti, M., Murphy, S., and Gutscher, M.-A.: Crustal structure of the Ionian basin and eastern Sicily margin: Results froma wide-angle seismic survey, J. Geophys. Res., 123, https://doi.org/10.1002/2017JB015312, 2018.

De Voogd, B., Truffert, C., Chamot-Rooke, N.. Huchon, P., Lallemant, S., and Le Pichon, X.: Two-ship deep seismic soundings in the basins of the Eastern Mediterranean Sea (Pasiphae cruise), Geophys. J. Int., 109 (3), pp. 536-552, 1992.

Dewey, J.F., Helman, M.L., Knott, S.D., Turco, E., and Hutton, D.H.W.: Kinematics of the western Mediterranean, Geological Society, London, Special Publications, 45, 265–283, http://dx.doi.org/10.1144/GSL.SP.1989.045.01.15, 1989.

Faccenna, C., Becker, T.W., Pio Lucente, F., Jolivet, L., and Rosetti, F.: History of subduction and back-arc extension in the Central Mediterranean, Geophys. J. Int., 145, 809-820, 2001.

Faccenna, C., Piromallo, C., Crespo-Blanc, A., and Jolivet, L.: Lateral slab deformation and the origin of the western Mediterranean arcs, Tectonics, 23, https://doi.org/10.1029/2002TC001488, 2004.

Faccenna, C., Becker, T.W., Auer, L., Billi, A., Boschi, L., Brun, J.P., Capitanio, F.A., Funiciello, F., Horvàth, F., Jolivet, L., Piromallo, C., Royden, L., Rossetti, F., and Serpelloni, E.: Mantle dynamics in the Mediterranean, Rev. Geophys., 52, 283–332, https://doi.org/10.1002/2013RG000444, 2014.

Ferrucci, F., Gaudiosi, G., Hirn, A., and Nicolich, R.: Ionian basin and Calabrian arc: some new elements from DSS Data, Tectonophysics, 195, 411-419, 1991.

Finetti, I. and Morelli, C.: Wide scale digital seismic exploration of the Mediterranean Sea, Boll. Geofis. Teor. Appl., 14, 291–342, 1972.

Finetti, I. and Morelli, C.: Geophysical exploration of the Mediterranean Sea, Boll. Geofis. Teor. Appl., 15, 263-341, 1973.

Finetti, I.: Geophysical study on the evolution of the Ionian Sea, in Wezel, F.C. eds. Sedimentary basins of Mediterranean margins. C.N.R. Italian Project of Oceanography, Bologna (Tecnoprint), 465-484, 1981.

Finetti, I.: Structure, stratigraphy and evolution of central Mediterranean. Bollettino di Geofisica Teorica ed Applicata, 24 (96), pp. 247-312, 1982.

Finetti, I., Lentini, F., Carbone, S., Catalano, S., Del Ben, A.: Il sistema Appennino Meridionale–Arco Calabro–Sicilia nel Mediterraneo Centrale: studio geologico-geofisico, Boll. Soc. geol. It., 115, 529-559, 1996.

Finetti, I.: The CROP profiles across the Mediterranean Sea (CROP MARE I and II), In Memorie descrittive della carta geologica d'Italia – CROP Atlas – Seismic Reflection Profiles of the Italian Crust, LXII, pp. 171–184, 2003.

Fruehn, J., Reston, T.J., Huene, R.v., and Bialas, J.: Structure of the Mediterranean Ridge accretionary complex from seismic velocity information, Marine Geology, 186, 43-58, 2001.

Fujie, G., Kasahara, J., Murase, K., Mochizuki, K., and Kaneda, Y.: Interactive analysis tools for the wide-angle seismic data for crustal structure study (Technical Report), Geophysical Exploration (BUTSURI-TANSA), Vol. 61, No. 1, pp26-33, 2008.

Gallais, F., Gutscher, M.A., Graindorge, D., Chamot-Rooke, N. and Klaeschen, D.: A Miocene tectonic inversion in the Ionian Sea (central Mediterranean): Evidence from multichannel seismic data, J. Geophys. Res.: Solid Earth, 116 (B12), https://doi.org/10.1029/2011JB008505, 2011.

Gallais, F., Gutscher, M.A., Klaeschen, D., and Graindorge, D.: Two-stage growth of the Calabrian accretionary wedge in the Ionian Sea (Central Mediterranean): Constraints from depth-migrated multichannel seismic data, Marine Geology, 326-328, p. 28-45, https://doi.org/10.1016/j.margeo.2012.08.006, 2012.

Gutscher, M.A., Kopp, H., Krastel, S., Bohrmann, G., Garlan, T., Zaragosi, S., Klaucke, I., Wintersteller, P., Loubrieu, B., LeFaou, Y., SanPedro, L., Dominguez, S., Rovere, M., Mercierde-Lepinay, B., Ranero, C., and Sallares, V.: Active tectonics of the Calabrian subduction revealed by new multi-beam bathymetric data and high-resolution seismic profiles in the Ionian Sea (Central Mediterranean), Eearth and Planet. Sci. Lett., 461, 61-72, https://doi.org/10.1016/j.epsl.2016.12.020, 2017.

Hestholm, S.O., Husebye, E.S., and Ruud, B.O.: Seismic wave propagation in complex crust-upper mantle media using 2-D finite-difference synthetics, Geophys. J. Int., 118, 3, 643-670, https://doi.org/10.1111/j.1365-246X.1994.tb03991.x, 1994.

Hieke, W., Hirschleber, H.B. and Dehghani, G.A.: The Ionian Abyssal Plain (central Mediterranean Sea): Morphology, subbottom structures and geodynamic history–an inventory, Marine Geophysical Researches, 24 (3-4), pp. 279-310, 2003.

Hsü K.J., Montadert, L., Bernoulli, D., Bizon, G., Cita, M.B., Erickson, A., Fabricius, F., Garrison, R.E., Kidd, R.B., Mélières, F., Müller, C., and Wright, R.C.: Site 374: Messina Abyssal Plain, in Hsü, K.J., Montadert, L. et al., Init. Rep. DSDP XLII, (part 1) 175–217, 1978.

Jiménez-Munt, I., and Negredo, A.: Neotectonic modelling of the western part of the Africa-Eurasia plate boundary: From the Mid-Atlantic ridge to Algeria, Earth Planet. Sci. Lett., 205, 257–271, https://doi.org/10.1016/S0012-821X(02)01045-2, 2003.

Le Breton, E., Handy, M.R., Molli, G., and Ustaszewski, K.: Post-20 Ma Motion of the Adriatic Plate: New Constraints From Surrounding Orogens and Implications for Crust-Mantle Decoupling, Tectonics, V36, I. 12, p. 3135-3154, https://doi.org/10.1002/2016TC004443, 2017.

Leister, K., Makris, J., Nicolich, R., and Rancke, D.: Crustal structure and crustal development in the Ionian Sea, Condenses Des Travaux Presentes Lors Du Xxxe Congres-Assemblee Pleniere de la C.I.E.S.M., Commission Internationale Pour l'Exploration Scientifique de la Mer Mediterranee, Paris, 30, 84, 1986.

Le Meur, D: Etude géophysique de la structure profonde et de la tectonique active de la partie occidentale de la Ride Méditerranéenne, 225 pp., Ph.D. thesis, Univ. Paris XI, Paris, 1997.

Locardi, E. and Nicolich, R.: Geodinamica del Tirreno e dell'Appennino centro-meridionale: la nuova carta della Moho, Mem. Soc. geol. It., 41, 121-140, 1988.

Makris, J., Nicolich, R., and Weigel, W.: A seismic study in the Western Ionian Sea, Annales Geophysicae, 4, 665-678.

Mantovani, E., D. Albarello, D. Babbucci, C. Tamburelli, and M. Viti, 2002. Trench-arc-back arc systems in the Mediterranean area: examples of extrusion tectonics, J. Virtual Explorer (online), 8, 131-147, 1986.

Micallef, A., Georgiopoulou, A., Mountjoy, J., Huvenne, V.A.I., Lo Iacono, C., Le Bas, T., Del Carlo, P., and Otero, D.C.: Outer shelf seafloor geomorphology along a carbonate escarpment: The eastern Malta Plateau, Mediterranean Sea, Continental Shelf Research, 131, 12-27, https://doi.org/10.1016/j.csr.2016.11.002, 2016.

Morelli, C., Gantar, G., and Pisani, M.: Bathymetry, gravity and magnetism in the Strait of Sicily and in the Ionian Sea, Boll. Geofis. Teor. Appl., 17, 39-58, 1975.

Nicolich, R.: Crustal structures from seismic studies in the frame of the European Geotraverse (southern segment) and Crop projects, in The Lithosphere in Italy, eds Boriani, A., M. Bonafede, G.B. Piccardo, G.B. Vai, Accad. Naz. Lincei, 80, 41-61, 1989.

Polonia, A., Torelli, L., Mussoni, P., Gasperini, L., Artoni, A., and Klaeschen, D.: The Calabrien Arc subduction complex in the Ionian Sea: Regional architecture, active deformation, and seismic hazard, Tectonics, 30, https://doi.org/10.1029/2010TC002821, 2011.

Reston, T.J., Huene, R.v., Dickmann, T., Klaeschen, D., and Kopp, H.: Frontal accretion along the western Mediterranean Ridge: the effect of Messinian evaporites on wedge mechanics and structural style, Marine Geology, 186, 59-82, 2002.

Roure, F., Casero, P., and Addoum, B.: Alpine inversion of the North African margin and delamination of its continental lithosphere. Tectonics, 31 (3), 2012.

Ryan W.B.F., Hsü, K.J., Cita, M.B., Dumitrica, P., Lort, J.M., Maync, W., Nesteroff, W.D., Pautot, G., Stradner, H., Wezel, F.C.: Initial Reports of the Deep Sea Drilling Project – Leg 13, V 13, Part 1, 1973.

Ryan W.B.F., Kastens, K.A., and Cita, M.B.: Geological evidence concerning compressional tectonics in the eastern Mediterranean, Tectonophysics, 86, 213-242, 1982.

~~Sage, F., Pontois, B., Mascle, J., and Basile, C.: Structure of oceanic crust adjacent to a transform margin segment: The Cote d'Ivoire Ghana transform margin, Geo-Marine Lett., 17, 31-39, https://doi.org/10.1007/PL00007204, 1997.~~

Sandwell, D.T., and Smith, W.H.F.: Marine gravity anomaly from Geosat and ERS 1 satellite altimetry, J. Geophys. Res., 102, 10039-10054, 1997.

Sandwell, D.T., Müller, R.D., Smith, W.H.F., Garcia, E., and Francis, R.: New global marine gravity model from CryoSat-2 and Jason-1 reveals buried tectonic structure, Science 346, 65, doi: 10.1126/science.1258213, 2014.

Scarascia, S. Lozej, A., and Cassinis, R.: Crustal structures of the Ligurian, Tyrrhenian and Ionian seas and adjacent onshore areas interpreted from wide-angle seismic profiles, Boll. geophys. Teor. Appl., 36, 5-19, 1994.

Sclater, J.G., Jaupart, C., and Galson, D.: The heat flow through ocean and continental crust and the heat loss of the Earth, Review of Geophysics, 18, 269-311, https://doi.org/10.1029/RG018i001p00269, 1980.

Sioni, S.: Mer Ionienne et Apulie depuis l'ouverture de l'Océan Alpin, Ph-D, Université de Bretagne Occidentale Brest, 241 pp, 1996.

Speranza, F., Minelli, L., Pignatelli, A. and Chiappini, M.: The Ionian Sea: The oldest in situ ocean fragment of the world? J. Geophys. Res.: Solid Earth, 117 (B12), 2012.

Spudich, P., and Orcutt. J.: Petrology and porosity of an oceanic crustal site: Results from wave form modeling of seismic refraction data, J. Geophys. Res., 85 (B3), 1409-1433, https://doi.org/10.1029/JB085iB03p01409, 1980.

Stampfli, G.M. Borel, G.D. Marchant, R., and Mosar, J.,: Western Alps geological constraints on western Tethyan reconstructions, Journal of the Virtual Explorer, 8, 77, 2002.

Talwani, M., Worzel, J.L., and Landisman, M.: Rapid gravity computations for two-dimensional bodies with application to the Mendocino submarine fracture zone, J. Geophys. Res., 64, 49-59, 1959.

Westbrook, G.K., and Reston, T.J.: The accretionary complex of the Mediterranean Ridge: tectonics, fluid flow and the formation of brine lakes – an introduction to the special issue of Marine Geology, Marine Geology, 186, 1-8, 2002.

White, R.S., McKenzie, D., and O'Nions, R.K.: Oceanic crustal thickness from seismic measurements and rare earth element inversions, J. Geophys. Res., 97, 19 683-19 715, 1992.

5   Zelt, C A., and Forsyth, D.A.: Modeling wide-angle seismic data for crustal structure: Southeastern Grenville Province, J. Geophys. Res., 99, 11,687–11,704, https://doi.org/10.1029/93JB02764, 1994.

Zelt, C.A., and Smith, R.B.: Seismic traveltime inversion for 2-D crustal velocity structure, Geophys. J. Int., 108, 16–34, https://doi.org/10.1111/j.1365-246X.1992.tb00836.x, 1992.
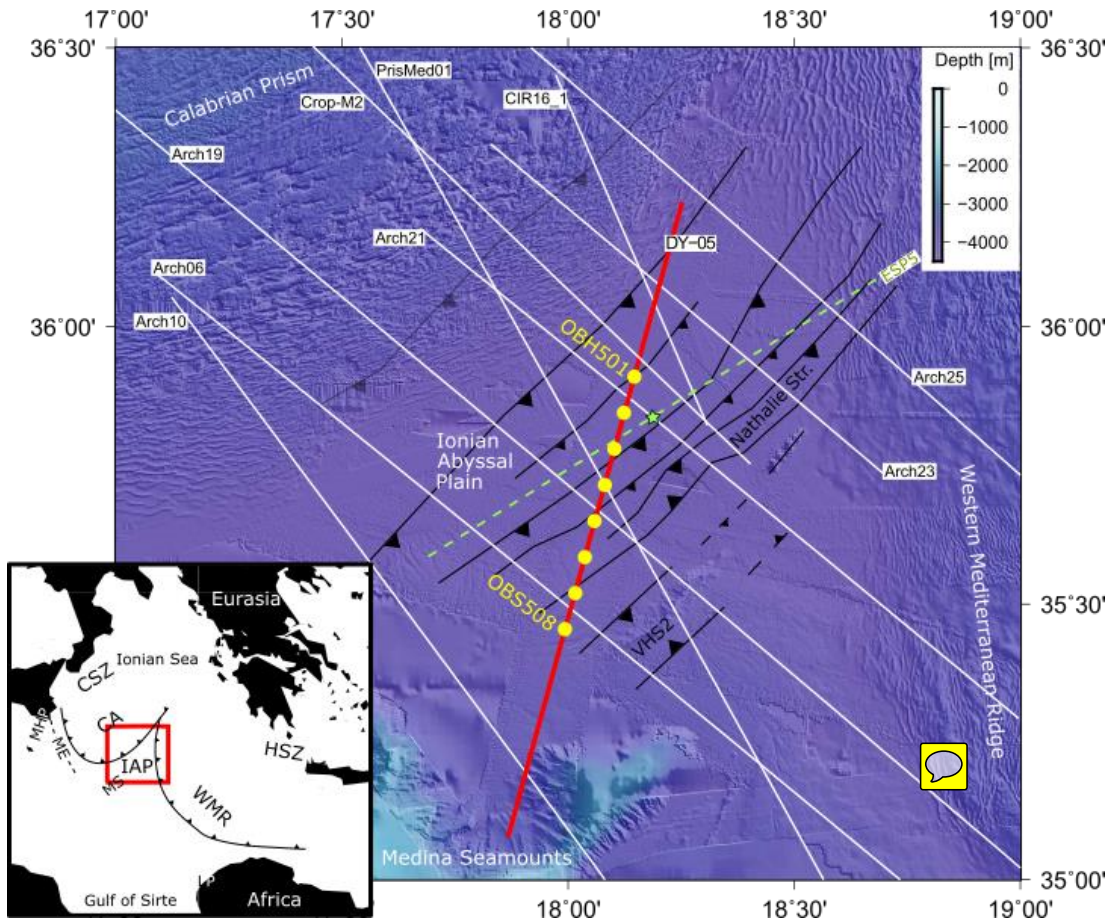
Figure 1: Map of the study area showing the location of the OBS profile DY-05 (red line) and the OBS locations (yellow dots). White lines present MCS data [Gallais et al., Polonia et al., 2011; 2011; 2012; Gutscher et al., 2017]. The green star marks the location of the ESP5 [De Voogd et al., 1992] and the location of DSDP Site 347 [Cita et al., 1978; Hsü et al., 1978] next to it. The ESP shotline is
5 **indicated by the green dashed line. Black lines indicate thrust faults [Gallais et al., 2011]. The black and white map shows the regional structures around the study area: IAP…Ionian Abyssal Plain, CSZ…Calabrian subduction zone, HSZ…Helenian subduction zone, WMR…Western Mediterranean Ridge, CA…Calabrian Arc, MS…Medina seamounts, ME…Malta Escarpment, MHP…Malta-Hyblean platform, LP…Libyan platform.**
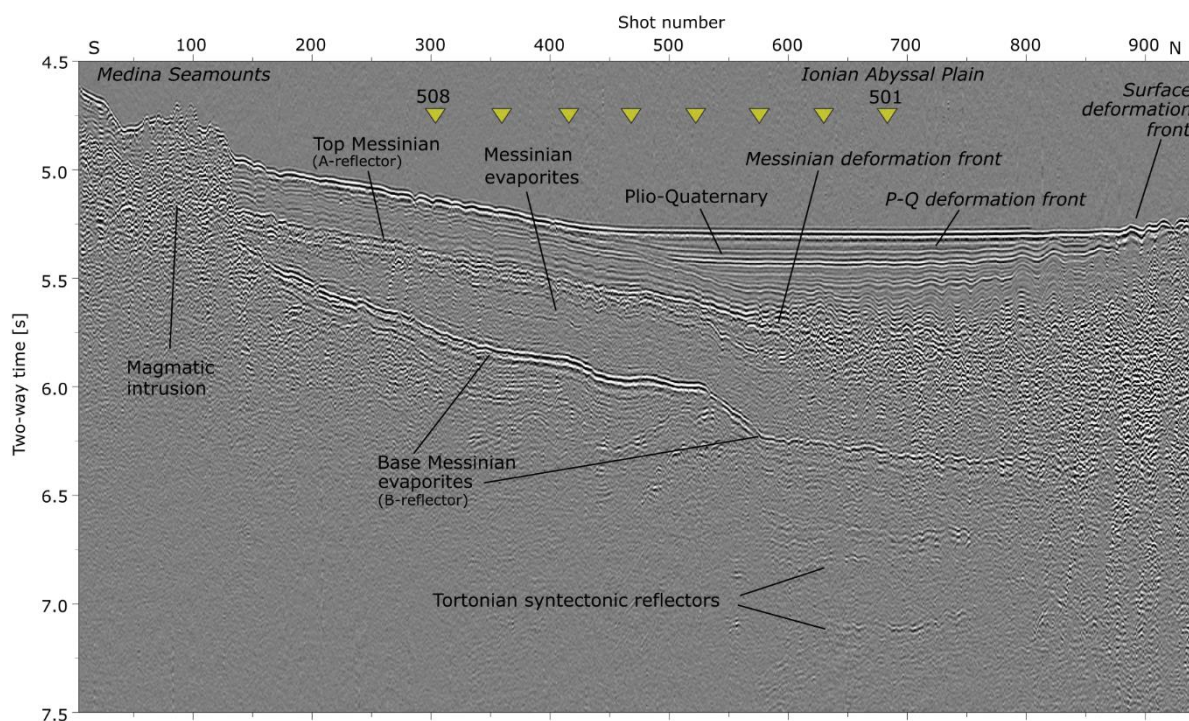
Figure 2: Stacked and band pass filtered (f=20,30,80,120 Hz) multi-channel data (MCS) along profile DY-05. Yellow triangles mark the OBS locations along the MCS profile.
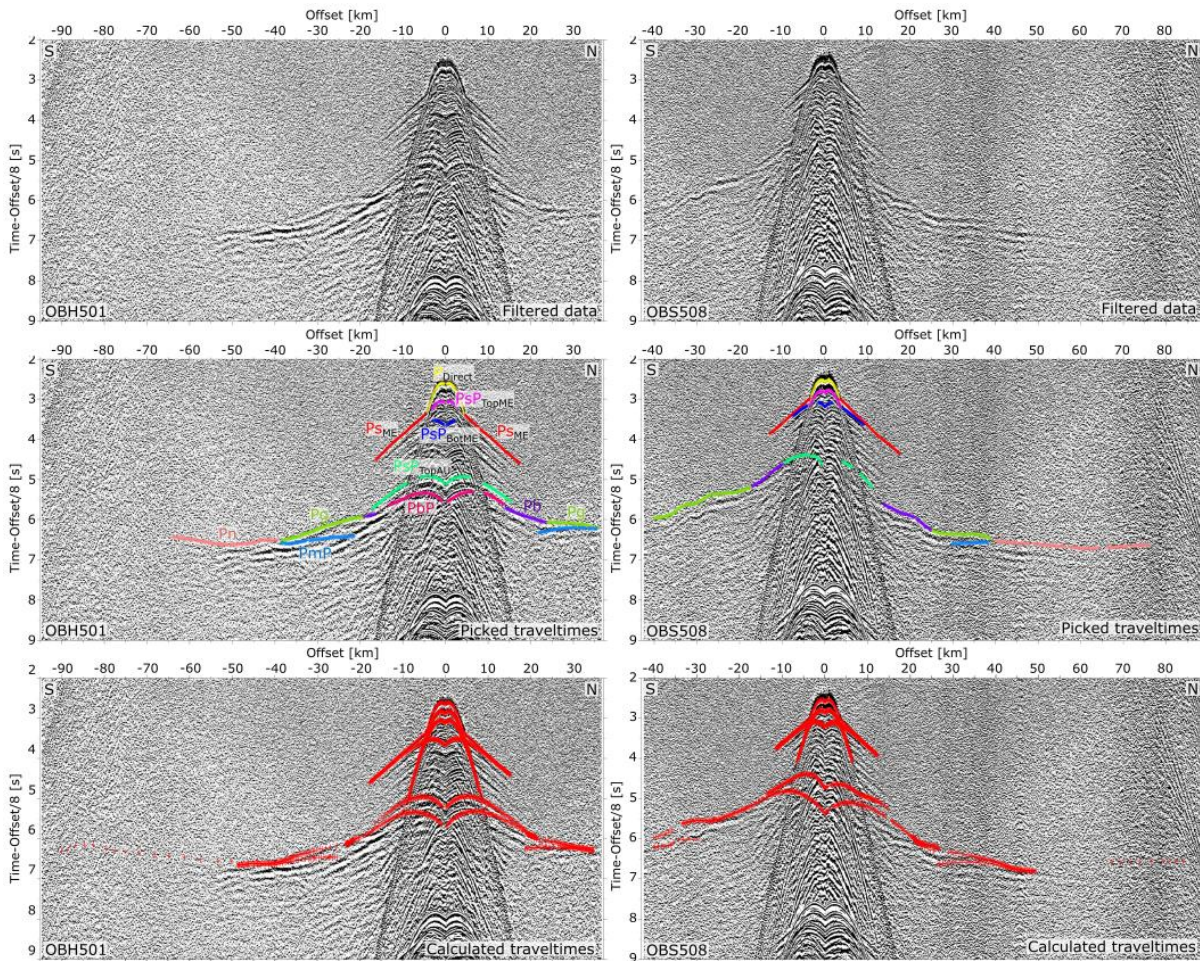
Figure 3: Seismic record sections of OBH501 and OBS508. Upper panel shows processed data. The middle panel shows the travel time picks used for the forward modelling (please refer to phase definitions in the text). Calculated travel times from the final model are displayed in the lower panel.
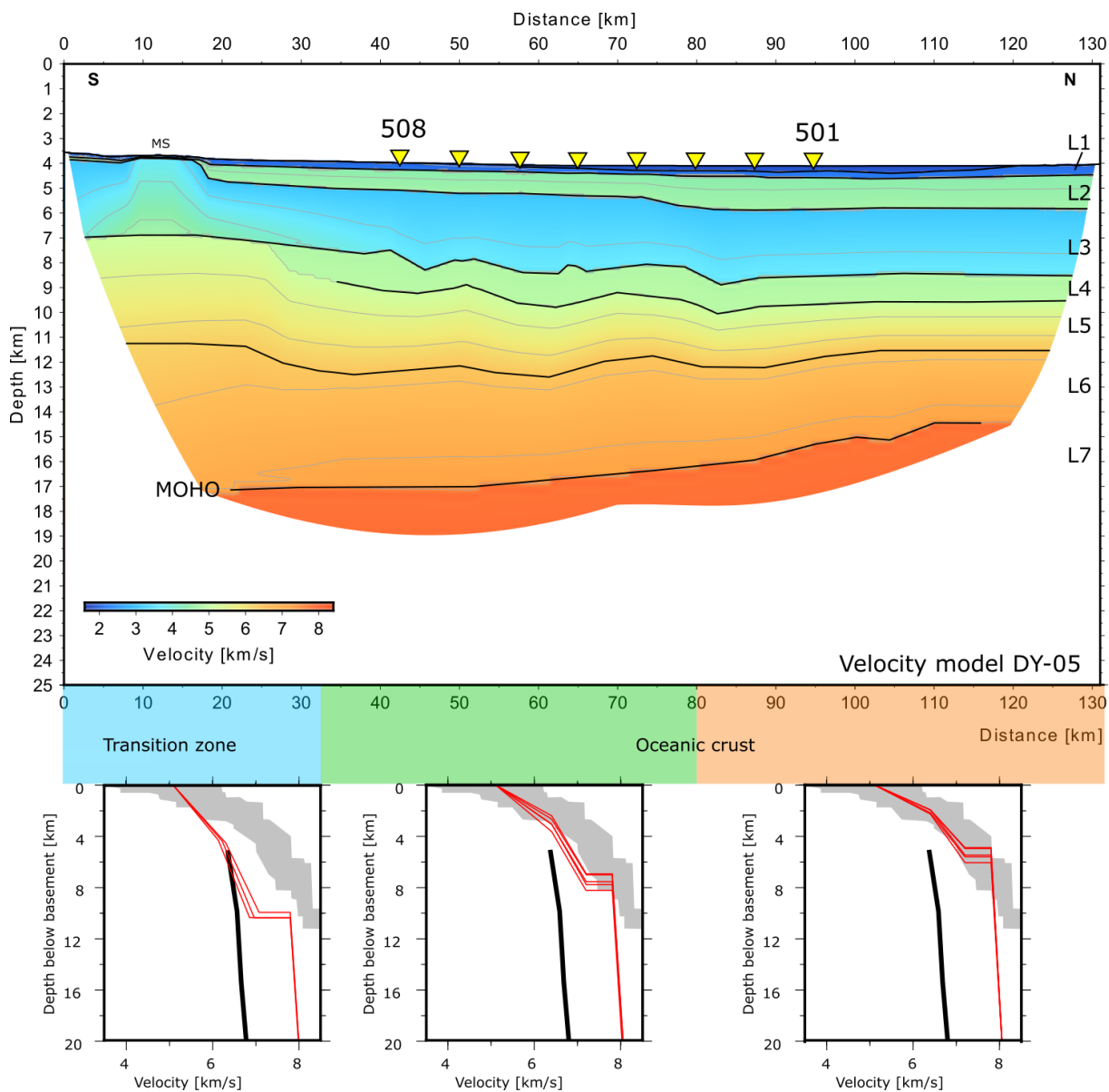
Figure 4: (a) Final velocity model for profile DY-05, gained from forward modelling. (b) Velocity-depth functions (red) starting at the basement, extracted from the final velocity model every 10 km. Observed velocities are compared to oceanic crust of similar age (grey area) [White et al., 1992] and continental crust (black line) [Christensen and Mooney, 1995].
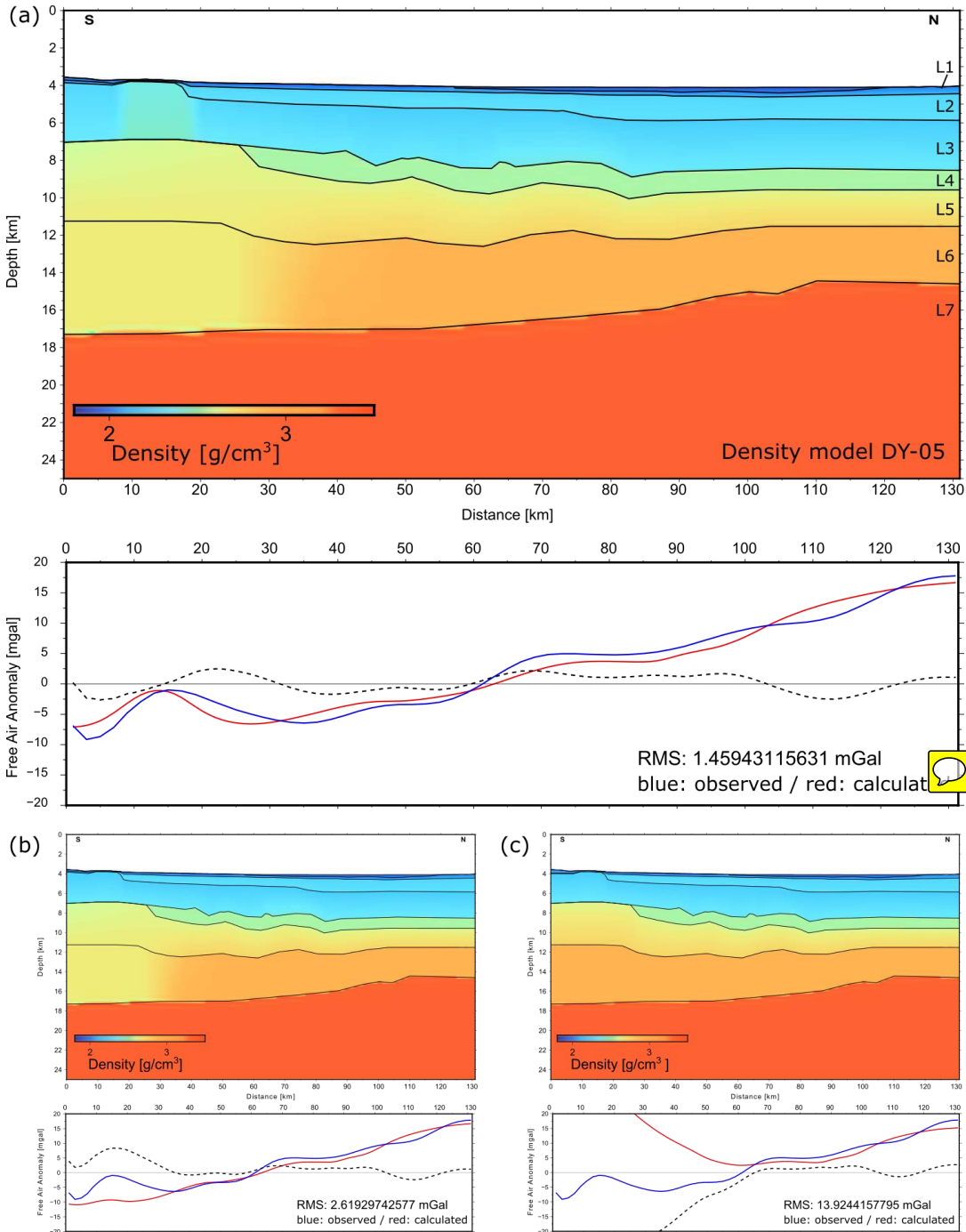
Figure 5: (a) The upper panel shows the density distribution calculated for profile DY-05 based on seismic velocities and minor adjustments to fit the observed FAA in the lower panel. **(b)** Case study for the local influence of the Medina Seamounts to the model response. **(c)** Case study for oceanic crust over the entire profile length. Black dashed line shows the residuum of the observed and calculated data.
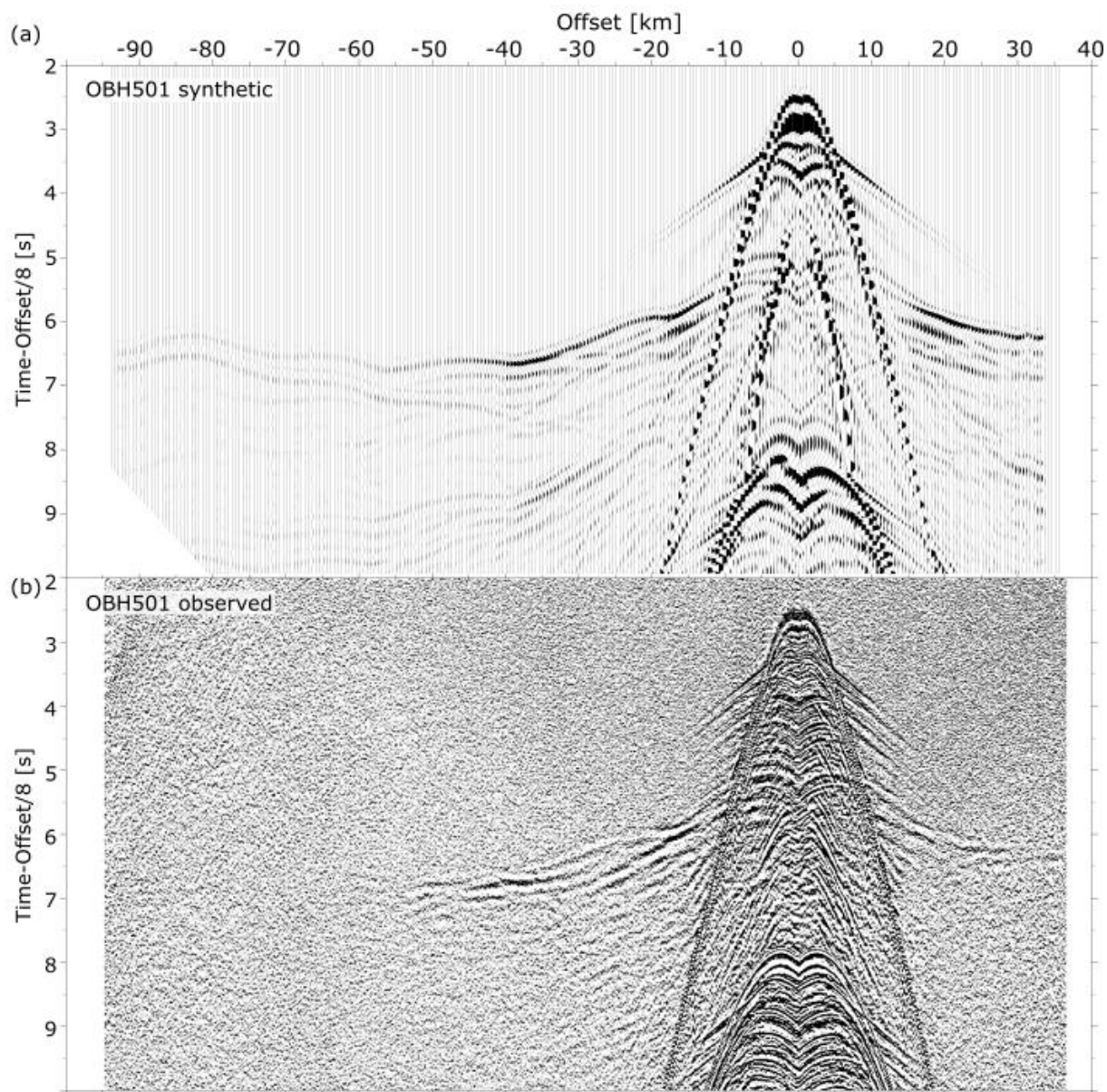
Figure 6: (a) Synthetic seismogram of OBH501 based on the final velocity model. (b) Original band pass filtered seismogram of OBH501.
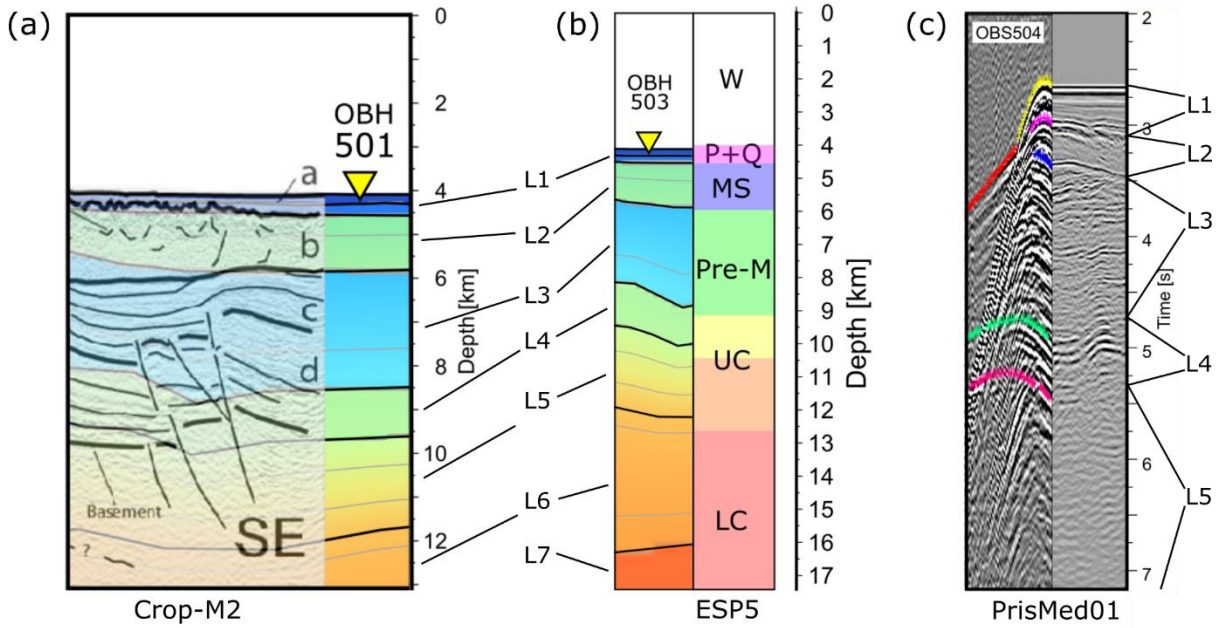
Figure 7: Comparison of the data and the final velocity model from this study with previous studies: (a) Crop-M2 [Polonia et al., 2011], (b) ESP5 [De Voogd et al. 1992], and (c) PrisMed01 [Gallais et al., 2011]. L1-L7 same layer convention as in the final velocity model.
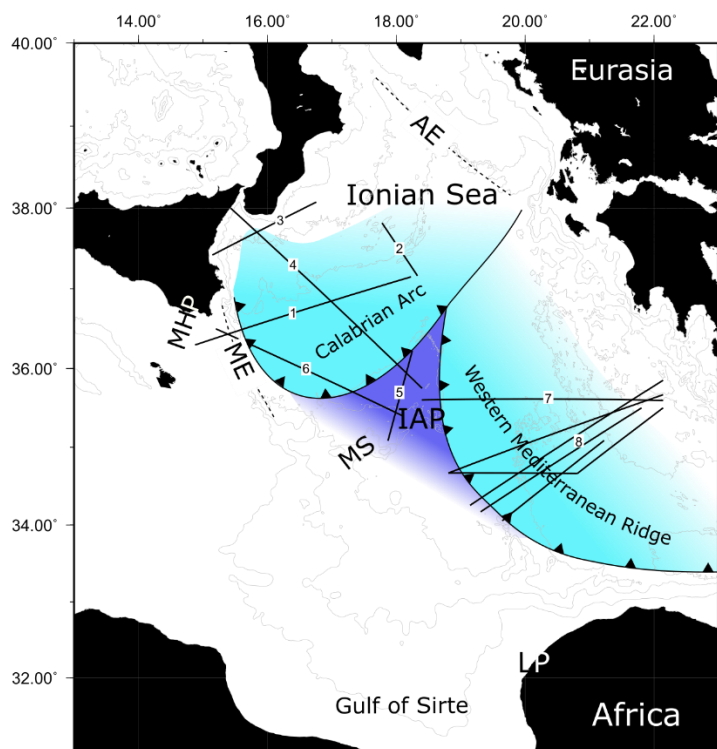
Figure 8: Dark blue marks presence of oceanic lithosphere below the seafloor in the Ionian Abyssal plain (undeformed portion) as determined by seismic studies. Light blue areas mark the extent of buried oceanic lithosphere below adjacent accretionary wedges as determined by seismic studies. Profile 1-5: M111; profile 6: Makris et al. [1986] and Finetti [2003] (part of Crop-M23A); profiles 7-8: IMERSE profiles [Fruehn et al., 2001; Westbrook and Reston, 2002; Reston et al., 2002]. AE… Apulian Escarpment. Further abbreviations are explained in Figure 1.